NEUROSCIENCE

Supramammillary regulation of locomotion and hippocampal activity

Jordan S. Farrell[1]*, Matthew Lovett-Barron[2,3], Peter M. Klein[1], Fraser T. Sparks[4,5,6], Tilo Gschwind[1], Anna L. Ortiz[1], Biafra Ahanonu[7,8], Susanna Bradbury[2], Satoshi Terada[4,5,6], Mikko Oijala[1], Ernie Hwaun[1], Barna Dudok[1], Gergely Szabo[1], Mark J. Schnitzer[7,9], Karl Deisseroth[2,9,10], Attila Losonczy[4,5,6], Ivan Soltesz[1]

Locomotor speed is a basic input used to calculate one's position, but where this signal comes from is unclear. We identified neurons in the supramammillary nucleus (SuM) of the rodent hypothalamus that were highly correlated with future locomotor speed and reliably drove locomotion when activated. Robust locomotion control was specifically identified in *Tac1* (substance P)–expressing (SuM^{Tac1+}) neurons, the activation of which selectively controlled the activity of speed-modulated hippocampal neurons. By contrast, *Tac1*-deficient (SuM^{Tac1-}) cells weakly regulated locomotion but potently controlled the spike timing of hippocampal neurons and were sufficient to entrain local network oscillations. These findings emphasize that the SuM not only regulates basic locomotor activity but also selectively shapes hippocampal neural activity in a manner that may support spatial navigation.

The ability to construct and access a mental map of one's environment during locomotion is an important adaptation to facilitate survival and is supported by tracking self-motion (*1*). Mammalian locomotion is intimately tied to the occurrence of 6- to 12-Hz hippocampal theta oscillations, such that the theta rhythm begins before the onset of self-generated motion and increases in amplitude with respect to speed (*2*–*6*). By temporally organizing the activity of place-coding neuronal assemblies into trajectories across past, present, and future locations, hippocampal theta oscillations are thought to subserve cognitive operations during spatial navigation (*5*–*10*). Tight coupling of theta waves to speed could be the result of shared neural circuitry between self-generated locomotion and theta control, providing a potential speed signal (*1*). Alternatively, speed could be derived from optic flow, vestibular input, or an efference copy from locomotor areas (*11*–*14*). Since the identification of speed-encoding neurons in brain areas that are thought to use a speed signal to calculate position (such as the hippocampus and entorhinal cortex) (*3*, *15*–*18*), research interest in understanding potential sources of speed input has grown.

The medial septum is critical for hippocampal theta activity and is functionally coupled

[1]Department of Neurosurgery, Stanford University, Stanford, CA, USA. [2]Department of Bioengineering, Stanford University, Stanford, CA, USA. [3]Neurobiology Section, Division of Biological Sciences, University of California, San Diego, CA, USA. [4]Department of Neuroscience, Columbia University, New York, NY, USA. [5]Kavli Institute for Brain Sciences, Columbia University, New York, NY, USA. [6]Mortimer B. Zuckerman Mind Brain Behavior Institute, Columbia University, New York, NY, USA. [7]Departments of Biology and Applied Physics, Stanford University, Stanford, CA, USA. [8]Department of Anatomy, University of California, San Francisco, CA, USA. [9]Howard Hughes Medical Institute, Stanford University, Stanford, CA, USA. [10]Department of Psychiatry and Behavioral Sciences, Stanford University, Stanford, CA, USA.
*Corresponding author. Email: jsfarrel@stanford.edu

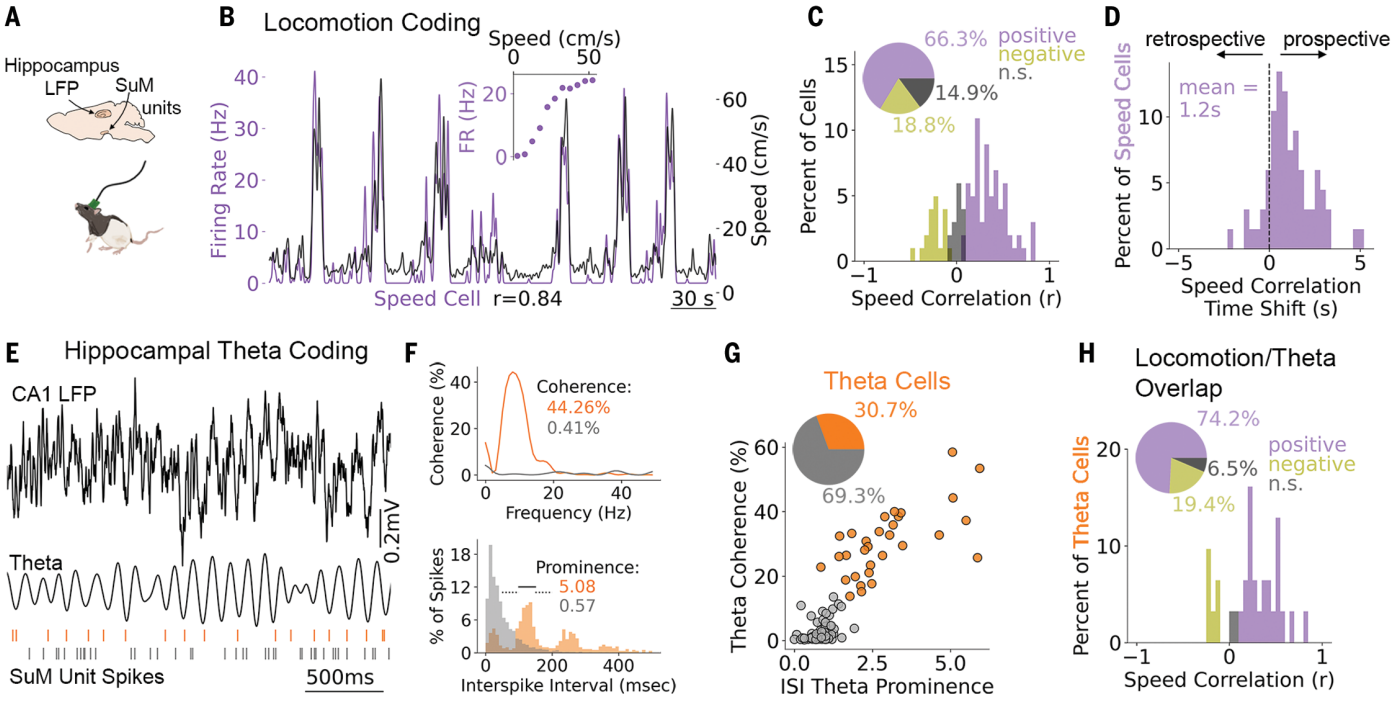

Fig. 1. SuM representation of speed and hippocampal theta oscillations. (**A**) Recording paradigm; data from unrestrained rats (*26*), reanalyzed here for speed- and theta-related investigations. (**B**) Example SuM unit (recorded by tetrodes) that is positively correlated with speed (i.e., a speed cell). The inset represents these data as a scatter plot. (**C**) Distribution of speed versus firing rate Pearson correlation coefficient (*r*) values. The pie chart shows the percentage of units for positive ($r = 0.36 \pm 0.023$, mean ± SEM), negative ($r = -0.24 \pm 0.024$), and nonsignificant (n.s.) cells ($r = 0.018 \pm 0.012$). (**D**) Distribution of temporal offsets for positive speed cells. SEM = 0.19. (**E**) Two example SuM unit spiking activities. The cell represented in orange shows phase-locked firing with respect to hippocampal theta oscillations, whereas the cell represented in gray does not. (**F**) Quantification of theta-related firing for two example units from (E). The top panel shows spike-field coherence; the bottom shows theta-rhythmic spiking. (**G**) Units were clustered into theta cells according to quantification from (F). ISI, interspike interval. (**H**) Distribution of speed scores among clustered theta cells from (G).

to locomotion (*3*, *19*–*21*), but other brain areas have been proposed to contribute to this oscillation. One such area is the supramammillary nucleus (SuM) of the posterior hypothalamus (*22*–*24*), which has recently been shown to have roles in arousal (*25*), spike-timing coordination (*26*), and identification of novelty (*27*). As a proposed theta controller, neural activity in the SuM is likely also related to locomotion, but this has not been systematically investigated. In addition to innervating the medial septum, the SuM has highly divergent outputs that target the midbrain, where locomotor commands are integrated, as well as regions involved in spatial navigation, including the hippocampus, entorhinal cortex, medial prefrontal cortex, nucleus reuniens, and claustrum (*28*). Thus, the SuM projects to theta, locomotor, and spatial navigation circuitry, but the functional relevance of this positioning remains poorly understood.

Using electrophysiological data from rats navigating a continuous alternation task for reward (*26*), we first investigated how the spiking activity of SuM neurons relates to locomotor speed and hippocampal theta oscillations (Fig. 1A). Similar to previous observations in the midbrain locomotor region (MLR) (*29*), we found a large proportion of SuM units with firing rates that were significantly coupled to locomotor speed, with the majority displaying a positive correlation (Fig. 1, B and C, and fig. S1, A, C, and D). Notably, SuM "speed cells" were more closely correlated with future speed (with an average offset of 1.2 s) than real-time speed (Fig. 1D and fig. S1, A and D). After adjusting for temporal offsets, the firing rates of 99% of SuM units were modulated by speed (fig. S1B). Most speed cells retained their correlation with immobility data withheld (fig. S1, E and F) and were more weakly coupled to acceleration than speed (fig. S2). SuM unit activity was also correlated to hippocampal theta amplitude in real time, but this was less accurately modeled than speed (fig. S3). Thus, SuM activity and locomotion are strongly coupled.

We then addressed whether speed-related neuronal activity is propagated to projection targets, because not all locally recorded SuM units are necessarily projection neurons. In vivo two-photon calcium imaging of SuM axon terminals that innervate the dentate gyrus (DG) and the CA2 region of the hippocampus was performed on head-fixed mice (fig. S4A). Indeed, speed-correlated activity in SuM axons was observed in both regions (fig. S4, B and C). Extensive collateralization of SuM axons was also determined (fig. S5) and may contribute to the similar proportion of positively and negatively correlated axons in both regions (fig. S4B).

Next, we examined the coupling between SuM action potentials and hippocampal theta waves (Fig. 1E). High coherence with hippocampal theta oscillations and theta-rhythmic spiking was observed for 30.7% of units (Fig. 1, F and G; see materials and methods). SuM theta cells typically fired near the trough of CA1 theta waves, with a slight prospective bias (fig. S6). Much like the overall SuM population, most SuM theta cells were positively correlated with locomotor speed (Fig. 1H).

To test the functional involvement of the SuM in locomotion and theta activity, we injected the SuM with recombinant adeno-associated virus (rAAV) to express the optogenetic proteins channelrhodopsin-2 (ChR2;

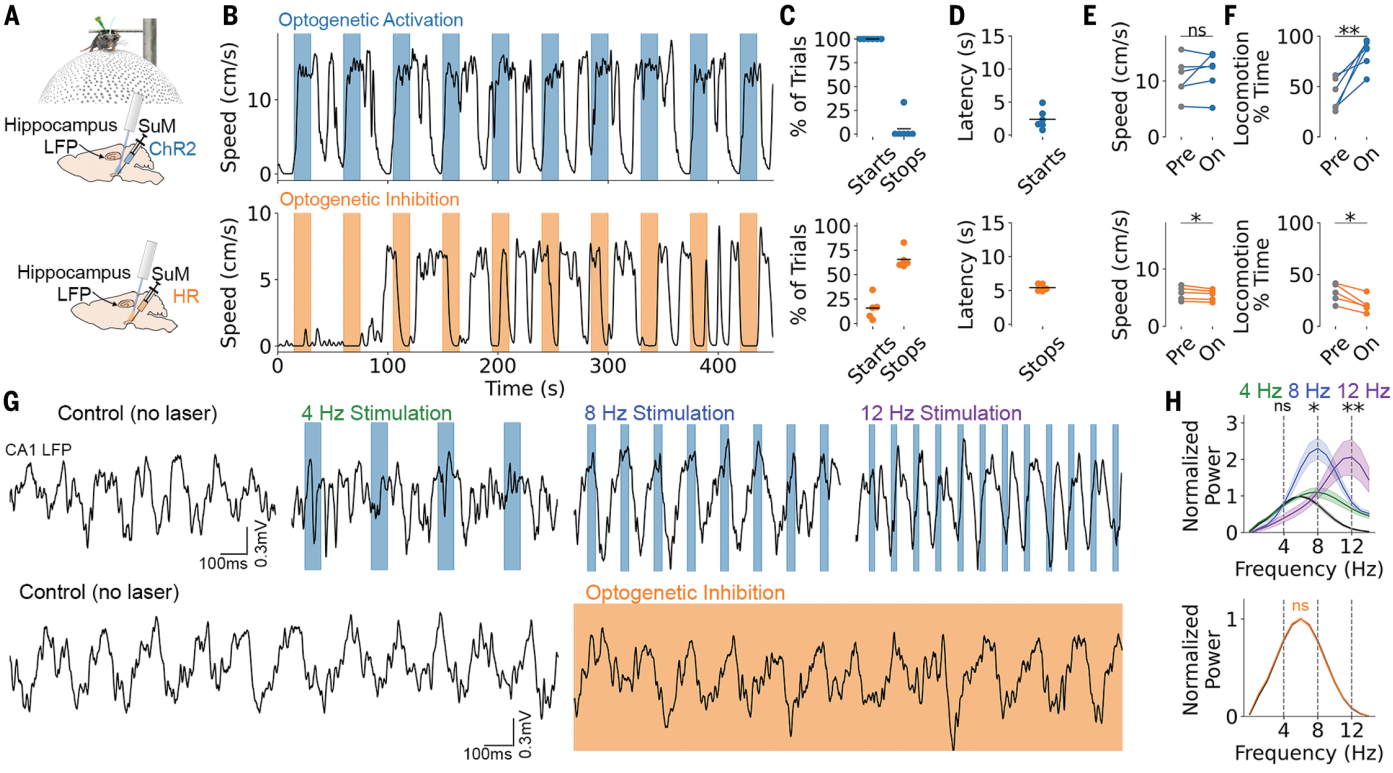

Fig. 2. Optogenetic SuM modulation controls locomotion and hippocampal LFP. (**A**) Pan-neuronal SuM activation with ChR2 (blue) or inhibition with HR (orange) in head-fixed mice on a floating ball. (**B**) Bidirectional locomotor effect with SuM activation (top) and inhibition (bottom). Colored bars denote "laser on" segments. (**C**) Percent of trials where locomotion was initiated or halted for ChR2 (top) and HR (bottom). (**D**) Latency of the start versus stop response. (**E**) Speed during locomotor epochs before (Pre) and during (On) light delivery. ChR2, $t_5 = -1.14$, $P = 0.31$; HR, $t_4 = 3.07$, $P = 0.037$. (**F**) Percent of time spent locomoting before (Pre) and during (On) light delivery. ChR2, $t_5 = -4.84$, $P = 0.0047$; HR, $t_4 = 4.60$, $P = 0.010$. (**G**) (Top) Optogenetic activation at 4, 8, or 12 Hz compared with no laser control. Blue bars denote laser on. (Bottom) Optogenetic inhibition (orange shading) versus no laser control. The scale bar applies across rows. (**H**) Quantification of power spectrum changes normalized to no laser control. (Top) ChR2: 4-Hz power at 4-Hz stimulation, $t_5 = 0.86$, $P = 0.43$; 8-Hz power at 8-Hz stimulation, $t_5 = 5.18$, $P = 0.0035$; 12-Hz power at 12-Hz stimulation, $t_5 = 3.99$, $P = 0.010$. (Bottom) HR: $t_4 = 0.043$, $P = 0.97$. Data are mean ± SEM. ns, not significant. *$P < 0.05$, **$P < 0.01$.

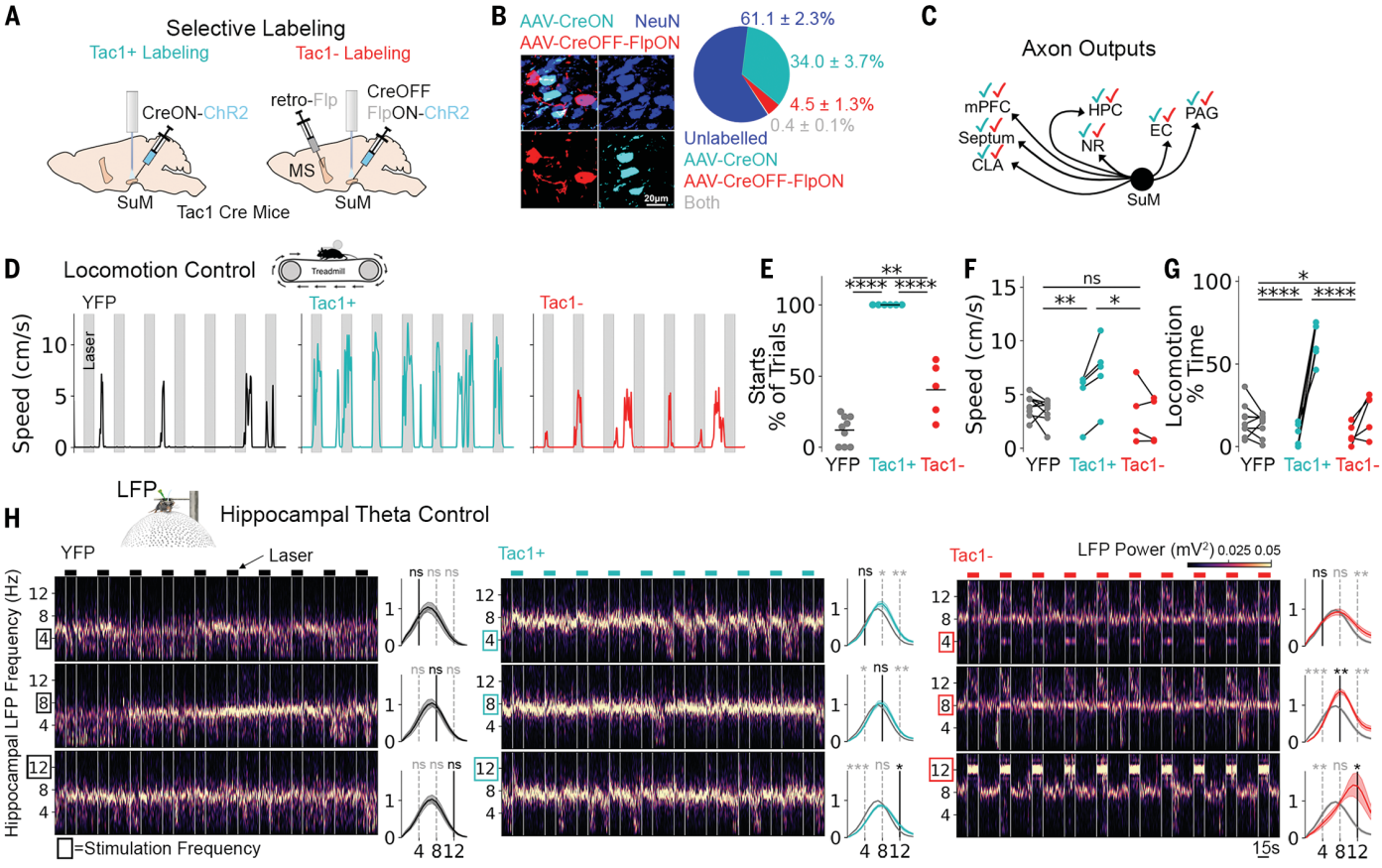

Fig. 3. Cell type dependence of locomotion initiation and LFP entrainment. (**A**) Labeling strategy to target mutually exclusive populations according to the presence or absence of *Tac1*. MS, medial septum. (**B**) Investigation of labeling specificity. (Left) Image showing AAV-labeled *Tac1*+ (CreON) and *Tac1*− cells (CreOFF-FlpON) among other NeuN+ cells in the SuM. (Right) Quantification. (**C**) Schematic showing checkmarks of each color (cyan, SuM^{Tac1+}; red, SuM^{Tac1-}) if axons were found in SuM target regions (see fig. S9). mPFC, medial prefrontal cortex; CLA, claustrum; HPC, hippocampus; NR, nucleus reuniens; EC, entorhinal cortex; PAG, periaqueductal gray. (**D**) Representative locomotor activity during optogenetic activation at 8 Hz. YFP, yellow fluorescent protein. (**E**) Percent of trials with locomotion initiation. Analysis of variance (ANOVA) $F_{2,17} = 103.6$, $P < 0.0001$, Tukey post hoc test. (**F**) Locomotor speed before (left dot) versus during (right dot) light delivery, connected by a line for each mouse. ANOVA was performed to determine group differences on changes in speed (before versus during light delivery). $F_{2,15} = 7.2$, $P = 0.0064$, Tukey post hoc test. (**G**) Percent of time locomoting before (left dot) versus during (right dot) light delivery. Differences in response change were assessed by ANOVA. $F_{2,17} = 57.8$, $P < 0.0001$, Tukey post hoc test. (**H**) Optogenetic stimulation in head-fixed mice on a floating ball at 4, 8, or 12 Hz. Spectrogram (left) and power spectral density changes [right; off (light gray) versus on (black, YFP; cyan, Tac1+; red, Tac1−)] for each condition (columns) at each frequency (rows). Paired *t* tests performed in light-off versus light-on conditions. ns, not significant. *$P < 0.05$, **$P < 0.01$, ***$P < 0.001$, ****$P < 0.0001$.

excitatory) or halorhodopsin (HR; inhibitory) under control of a pan-neuronal promoter (Fig. 2, A and G). Light activation of ChR2 drove locomotion in 100% of trials, with an average latency of 2.4 ± 0.6 s in head-fixed mice (Fig. 2, B to F). Locomotion lagged behind an increase in theta amplitude (fig. S7), which is consistent with prospective encoding of speed but real-time encoding of theta amplitude (Fig. 1D versus fig. S3A). The frequency of laser pulses reliably entrained hippocampal local field potential (LFP) at 8 and 12 Hz (Fig. 2, G and H), similar to previous optogenetic manipulations in the medial septum (*3*, *4*, *20*, *21*). Most CA1 neurons (94%) were entrained by laser pulses; however, the preferred firing phase shifted considerably from spontaneous theta activity (fig. S8). Optogenetic inhibition with HR halted locomotion on 65.6 ± 0.6% of trials, with a latency of 5.4 ± 0.2 s (Fig. 2, B to F). Consistent with previous studies (*26*, *30*), SuM inhibition did not alter hippocampal theta rhythms during locomotion (Fig. 2, G and H). Thus, optogenetic manipulation of the SuM robustly and bidirectionally controls locomotion but does not inhibit spontaneous hippocampal theta waves, despite robust spike and LFP entrainment with ChR2.

Considering the heterogeneity of SuM cell types (*31*), we then determined whether locomotion control and spike and LFP entrainment were dependent on cell type. A subset of SuM neurons express substance P, encoded by the *Tac1* gene, and project to the hippocampus and other regions (*32*). Using the Tac1-Cre mouse line, we targeted two mutually exclusive populations. *Tac1*-expressing (SuM^{Tac1+}) neurons were labeled with a CreON rAAV, whereas a smaller population of *Tac1*-deficient (SuM^{Tac1-}) projection neurons were labeled with an intersectional approach using a CreOFF-FlpON rAAV (*33*), facilitated by a retrograde rAAV carrying Flp in the medial septum (Fig. 3, A and B). The axon outputs of both cell populations were similar, innervating the known and expected SuM target regions (Fig. 3C and fig. S9). However, SuM^{Tac1+} and SuM^{Tac1-} cells had different intrinsic properties (fig. S10). Cell types were further differentiated by the non-uniform axon innervation pattern of the DG granule cell layer (fig. S11C) and increased vesicular γ-aminobutyric acid (GABA) transporter content of SuM^{Tac1-} cells (fig. S11, A and B), consistent with previously identified GABA and glutamate co-releasing SuM cells (*34*). Functionally, SuM^{Tac1+} cell stimulation robustly drove locomotion in 100% of trials (Fig. 3, D to G) but did not entrain hippocampal LFP (Fig. 3H). This locomotion was relatively slow and steady with an alternating

stepping pattern (movie S1), consistent with exploratory locomotion and distinct from fight or flight responses seen with stimulation of other hypothalamic areas (*35*). By contrast, activation of SuM^{Tac1-} cells weakly controlled locomotion (Fig. 3, D to G) but precisely controlled the frequency of hippocampal LFP at 8 and 12 Hz (Fig. 3H).

Given the robust control of movement initiation by SuM^{Tac1+} neuron stimulation, we further examined the role of this cell type in locomotion. Using two-photon calcium imaging in head-fixed mice running on a treadmill, we observed a high proportion of SuM^{Tac1+} cells for which activity was positively correlated with speed and that were active before locomotion onset (fig. S12). Similar results were obtained from *Tac1*+ cells in the ventral hypothalamus of zebrafish during swimming behavior, supporting evolutionary conservation of function (fig. S13). As with broad SuM inhibition, selective optogenetic inhibition of SuM^{Tac1+} neurons also suppressed locomotion in head-fixed mice (fig. S14). Finally, we examined potential SuM^{Tac1+} output pathways that reach the MLR, where the coordination of locomotor input and gait selection takes place (*36*). Using anterograde trans-synaptic tracing to label postsynaptic neurons (*37*), we found that midbrain periaqueductal gray neurons that specifically receive SuM^{Tac1+} input, in turn, project to the MLR (fig. S15).

Finally, we determined how SuM^{Tac1+} and SuM^{Tac1-} neurons alter firing rate and control spike timing of hippocampal neurons. Given the tight coupling of SuM^{Tac1+} cells to locomotion, we hypothesized that spontaneously speed-correlated hippocampal neurons would be particularly sensitive to SuM^{Tac1+} activation. On average, activation of both SuM cell types increased the firing rate of the hippocampal units during locomotion (Fig. 4B) and resulted in similar proportions of units with significant firing rate alterations (Fig. 4A). The effect of SuM^{Tac1+} stimulation, but not SuM^{Tac1-} stimulation, was indeed correlated to the magnitude of spontaneous speed modulation, such that the firing rates of positively correlated speed units increased, and negatively correlated cells decreased with optogenetic stimulation (Fig. 4B). We observed the opposite relationship with optogenetic inhibition of SuM^{Tac1+} cells (fig. S14E). Hippocampal speed cell firing rates were then modeled from speed and laser timing as inputs (Fig. 4C). Modeling firing rates during SuM^{Tac1+} stimulation produced considerably less error than modeling during SuM^{Tac1-} stimulation when laser timing was withheld (Fig. 4C), supporting the notion that the effect of SuM^{Tac1+} stimulation on locomotion and hippocampal speed cell firing rates are coupled.

At a subsecond time scale, we also determined whether hippocampal spike timing was altered relative to each laser pulse. Because SuM^{Tac1-} activation overrode spontaneous hippocampal theta waves and entrained LFP, we hypothesized that spike timing would be more affected by activation of this cell type. Indeed, SuM^{Tac1-} activation entrained spike timing in more units with a greater average effect (Fig. 4, D and E). Moreover, SuM^{Tac1-} activation increased the firing rate of most units in close proximity to the termination of each light pulse, whereas SuM^{Tac1+} activation had mixed responses (Fig. 4F and fig. S16). Unlike SuM^{Tac1-} stimulation, the effect of SuM^{Tac1+} stimulation depended on that unit's speed correlation, such that positively correlated hippocampal speed cells were more likely to fire shortly after laser pulse onset and negatively correlated cells were suppressed (Fig. 4G). A significant correlation between the magnitude of optogenetic entrainment and the magnitude of spontaneous theta entrainment was observed for activation of both cell types; however, the linear fit slope was twice the value for SuM^{Tac1-} activation (Fig. 4H). Lastly, the preferred firing phase relative to hippocampal theta activity was more perturbed by SuM^{Tac1-} cell activation (fig. S17).

The finding that SuM^{Tac1-} cells potently regulate hippocampal spike timing and are sufficient to entrain LFP is notable, given the lack of effect of SuM inhibition on spontaneous hippocampal theta oscillations. However, others have reported no change in hippocampal theta activity with SuM inhibition and lesions

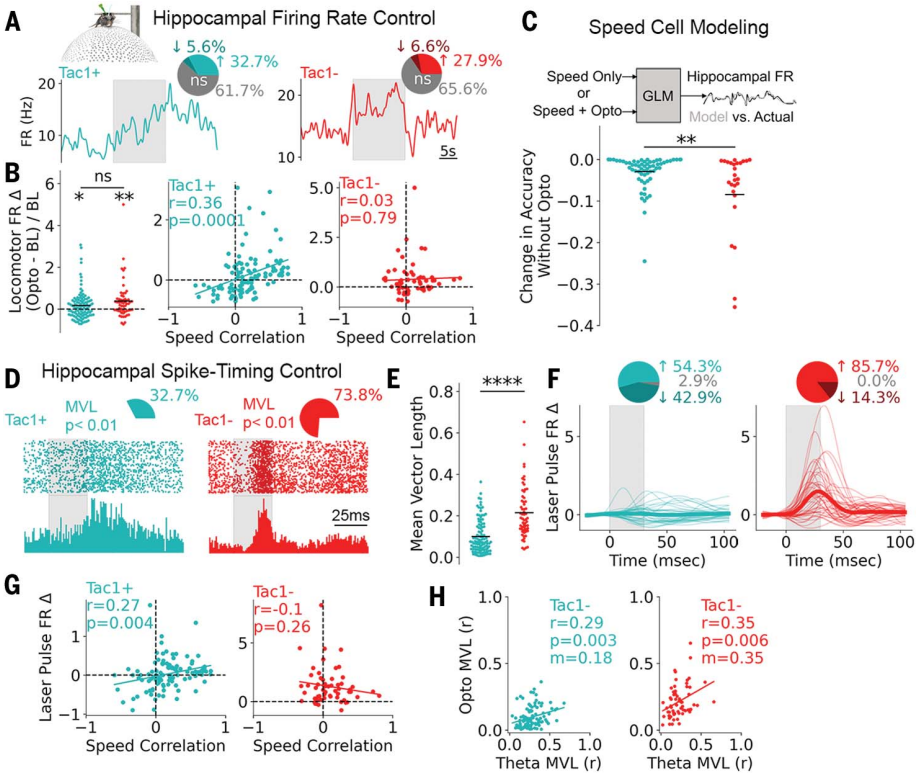

Fig. 4. Hippocampal populations are differentially regulated by SuM cell types. (**A**) Data were obtained from head-fixed mice on a floating ball. Mean firing rate (FR) changes from two example hippocampal cells during SuM^{Tac1+} or SuM^{Tac1-} optogenetic activation (gray shaded area). Pie charts display the proportion of units with significantly altered locomotor firing rates. (**B**) Locomotor firing rate change for light-on versus light-off conditions (one-sample *t* test: SuM^{Tac1+}, t_{105} = 2.56, P = 0.012; SuM^{Tac1-}, t_{57} = 3.28, P = 0.0017; between sample *t* test: t_{162} = 1.69, P = 0.09) and as a function of speed correlation (calculated while laser is off). The *y*-axis label applies to all panels. BL, baseline. (**C**) Generalized linear model of hippocampal speed cell firing rate, with two sets of input [speed only versus speed + optogenetic input (opto)]. The plot shows the change in modelling accuracy when optogenetic information was withheld (t_{89} = 3.28, P = 0.0015). (**D**) Hippocampal spike raster plots with histograms aligned to laser pulses (gray bar) during 8-Hz stimulation. Pie charts show the proportion of units with significantly laser-modulated spike distributions. MVL, mean vector length. (**E**) Quantification of nonuniform spike distributions from (D). t_{166} = 7.39, P = 6.8 × 10^{12}. (**F**) Smoothed spike histograms of significantly laser-modulated cells. Thin lines represent individual cells; the thick line represents the mean. Pie charts show the directionality of modulation. (**G**) Laser pulse–triggered firing rate change plotted against cells' speed correlations (calculated while laser is off). (**H**) Firing rate modulation by spontaneous theta versus optogenetic laser pulses. m, slope. Lines in (B), (G), and (H) represent linear fits.

(*26*, *30*), despite substantial effects with SuM activation (*31*). Recent work demonstrated that a subpopulation of SuM units increase their activity under novel conditions (*27*). SuM cells from this previous study have several characteristics that overlap with SuM^{Tac1-} cells, including the nonuniform axonal innervation pattern and mixed neurotransmitter phenotype in the DG (*34*). In another study, optogenetic inhibition of the SuM affected theta-range spike timing in SuM-connected structures, but only at the decision point of the maze (*26*). Thus, SuM^{Tac1-} cells may be most influential to hippocampal network patterns in particularly salient situations, with little contribution to the mechanisms that underlie spontaneous theta waves. Consistent with this model, SuM^{Tac1-} activation caused a considerable shift in firing phase preferences from spontaneously generated theta rhythm, highlighting potentially different underlying mechanisms for SuM^{Tac1-}-evoked versus spontaneous theta oscillations.

These data also advance our understanding of the SuM's in role in locomotion and identify a cell type with functional properties relevant to spatial navigation. In addition to the tight coupling of SuM^{Tac1+} activity to speed, we found that SuM^{Tac1+} activation robustly drove locomotion while selectively regulating the activity of speed-sensitive hippocampal neurons. These data raise the possibility that SuM^{Tac1+} neurons have a role in distributing a speed signal throughout the SuM's many axon-termination sites and complement recent work outlining a speed-relaying pathway from the MLR to the entorhinal cortex via the septum (*38*). Given that SuM^{Tac1+} cells encode future speed, the SuM may provide its synaptic partners with intended speed, whereas executed speed is propagated from the MLR. Thus, the SuM may support a role in planning and error correction during locomotion by broadcasting a future speed signal.

REFERENCES AND NOTES

1. J. O'Keefe, L. Nadel, *The Hippocampus as a Cognitive Map* (Clarendon Press, 1978).
2. C. H. Vanderwolf, *Electroencephalogr. Clin. Neurophysiol.* **26**, 407–418 (1969).
3. T. C. Foster, C. A. Castro, B. L. McNaughton, *Science* **244**, 1580–1582 (1989).
4. F. Fuhrmann *et al.*, *Neuron* **86**, 1253–1264 (2015).
5. L. L. Colgin, *Annu. Rev. Neurosci.* **36**, 295–312 (2013).
6. G. Buzsáki, *Rhythms of the Brain* (Oxford Univ. Press, 2006).
7. J. O'Keefe, M. L. Recce, *Hippocampus* **3**, 317–330 (1993).
8. W. E. Skaggs, B. L. McNaughton, M. A. Wilson, C. A. Barnes, *Hippocampus* **6**, 149–172 (1996).
9. E. Pastalkova, V. Itskov, A. Amarasingham, G. Buzsáki, *Science* **321**, 1322–1327 (2008).
10. M. R. Mehta, A. K. Lee, M. A. Wilson, *Nature* **417**, 741–746 (2002).
11. W. M. Sheeran, O. J. Ahmed, *Neurosci. Biobehav. Rev.* **108**, 821–833 (2020).
12. R. G. K. Munn, C. S. Mallory, K. Hardcastle, D. M. Chetkovich, L. M. Giocomo, *Nat. Neurosci.* **23**, 239–251 (2020).
13. J. A. Pérez-Escobar, O. Kornienko, P. Latuske, L. Kohler, K. Allen, *eLife* **5**, e16937 (2016).
14. M. G. Campbell *et al.*, *Nat. Neurosci.* **21**, 1096–1106 (2018).
15. M. Iwase, T. Kitanishi, K. Mizuseki, *Sci. Rep.* **10**, 1407 (2020).
16. E. Kropff, J. E. Carmichael, M. B. Moser, E. I. Moser, *Nature* **523**, 419–424 (2015).
17. D. Justus *et al.*, *Nat. Neurosci.* **20**, 16–19 (2017).
18. J. R. Hinman, M. P. Brandon, J. R. Climer, G. W. Chapman, M. E. Hasselmo, *Neuron* **91**, 666–679 (2016).
19. J. D. Green, A. A. Arduini, *J. Neurophysiol.* **17**, 533–557 (1954).
20. H. Dannenberg *et al.*, *J. Neurosci.* **35**, 8394–8410 (2015).
21. I. Zutshi *et al.*, *Curr. Biol.* **28**, 1179–1188.e3 (2018).
22. I. J. Kirk, N. McNaughton, *Neuroreport* **2**, 723–725 (1991).
23. I. J. Kirk, S. D. Oddie, J. Konopacki, B. H. Bland, *J. Neurosci.* **16**, 5547–5554 (1996).
24. B. Kocsis, R. P. Vertes, *J. Neurosci.* **14**, 7040–7052 (1994).
25. N. P. Pedersen *et al.*, *Nat. Commun.* **8**, 1405 (2017).
26. H. T. Ito, E. I. Moser, M. B. Moser, *Neuron* **99**, 576–587.e5 (2018).
27. S. Chen *et al.*, *Nature* **586**, 270–274 (2020).
28. R. P. Vertes, *J. Comp. Neurol.* **326**, 595–622 (1992).
29. A. M. Lee *et al.*, *Neuron* **83**, 455–466 (2014).
30. J. S. Thinschmidt, G. G. Kinney, B. Kocsis, *Neuroscience* **67**, 301–312 (1995).
31. W. X. Pan, N. McNaughton, *Prog. Neurobiol.* **74**, 127–166 (2004).
32. T. Ino *et al.*, *Neurosci. Lett.* **90**, 259–264 (1988).
33. L. E. Fenno *et al.*, *Nat. Methods* **11**, 763–772 (2014).
34. F. Billwiller *et al.*, *Brain Struct. Funct.* **225**, 2643–2668 (2020).
35. Y. Li *et al.*, *Neuron* **97**, 911–924.e5 (2018).
36. V. Caggiano *et al.*, *Nature* **553**, 455–460 (2018).
37. B. Zingg *et al.*, *Neuron* **93**, 33–47 (2017).
38. M. M. Carvalho *et al.*, *Cell Rep.* **32**, 108123 (2020).

ACKNOWLEDGMENTS

The authors thank H. Ito, E. Moser, and M.-B. Moser for generously sharing a previously published dataset for reanalysis for the specific purposes of this study and for providing comments on the manuscript. The authors also thank R. Kumar and S. Felong for technical assistance. **Funding:** This work was supported by a Canadian Institutes of Health Research postdoctoral fellowship (J.S.F.); National Institute of Mental Health (NIMH) K99MH11284002 (M.L.-B.); an American Epilepsy Society (AES) Junior Investigator Award (F.T.S.); Stanford Epilepsy Training Grant 5T32NS007280 funded by the National Institute of Neurological Disorders and Stroke (NINDS) (P.M.K. and E.H.); a Swiss National Science Foundation Postdoctoral Fellowship (T.G.); National Science Foundation Fellowship DGE-114747 (B.A.); a HHMI Gilliam Fellowship for Advanced Study (B.A.); Gates Millennium Scholarship (B.A.); a Japan Society for the Promotion of Science (JSPS) Overseas Fellowship (S.T.); an AES Postdoctoral Fellowship (B.D.); NINDS K99NS117795 (B.D.); National Institute of Health (NIH) 1U19NS104590 (I.S., A.L., and M.J.S.); NIMH 1R01MH124047 and 1R01MH124867 (A.L.); the Kavli Foundation (A.L.); and the NIH, NSF, Gatsby, Fresenius, and NOMIS Foundations (K.D.).

Author contributions: Conceptualization: J.S.F. and I.S. Methodology: B.A., M.O., and G.S. Investigation: J.S.F., M.L.-B., P.M.K., F.T.S., T.G., A.L.O., and S.B. Formal analysis: J.S.F. M.L.-B., P.M.K., F.T.S., T.G., S.T., M.O., E.H., and B.D. Funding acquisition: M.J.S., K.D., A.L., and I.S. Supervision: M.J.S., K.D., A.L., I.S. Writing – original draft: J.S.F. and I.S. Writing – review & editing: all authors. **Competing interests:** M.J.S. is a scientific cofounder of Inscopix. GRIN lenses used in this studied were purchased from Inscopix. **Data and materials availability:** Code used in this study came from publicly available resources referenced in the materials and methods. Parts of the raw datasets and additional custom code are openly available at solteszlab.com/datasets and will continue to be formatted and uploaded.

SUPPLEMENTARY MATERIALS

science.org/doi/10.1126/science.abh4272
Materials and Methods
Figs. S1 to S17
References (*39*–*65*)
Movie S1

View/request a protocol for this paper from *Bio-protocol*.

11 March 2021; accepted 29 October 2021
10.1126/science.abh4272

Science

Supramammillary regulation of locomotion and hippocampal activity

Jordan S. FarrellMatthew Lovett-BarronPeter M. KleinFraser T. SparksTilo GschwindAnna L. OrtizBiafra AhanonuSusanna BradburySatoshi TeradaMikko OijalaErnie HwaunBarna DudokGergely SzaboMark J. SchnitzerKarl DeisserothAttila LosonczyIvan Soltesz

Science, 374 (6574), • DOI: 10.1126/science.abh4272

Locomotion-related signals in the brain

To calculate where we are in space, continuous knowledge of one' s speed is necessary. How does the brain know how fast the body is traveling during locomotion? Using in vivo calcium imaging, electrophysiology, optogenetics, cell tracing, and histology, Farrell *et al*. identified neurons in the rodent supramammillary nucleus of the hypothalamus that encode future locomotor speed and potently drive locomotion when stimulated. Because these locomotor neurons have extensive axons in brain areas that support spatial navigation, this cell type distributes this information selectively to areas that require knowledge of speed. This nucleus is functionally positioned between input from a higher-order cognitive center and the downstream midbrain where locomotor nuclei reside. —PRS

Science (ISSN) is published by the American Association for the Advancement of Science. 1200 New York Avenue NW, Washington, DC 20005. The title *Science* is a registered trademark of AAAS.